Journal of Bioscience and Bioengineering
VOL. 128 No. 2, 218–225, 2019

ELSEVIER

www.elsevier.com/locate/jbiosc

Micro and ultrastructural changes monitoring during decellularization for the generation of a biocompatible liver

Ebtehal Ahmed,[1] Tarek Saleh,[1] Lina Yu,[1] Ho-Hyun Kwak,[1] Byeong-Moo Kim,[2] Kyung-Mee Park,[3] Yun-Suk Lee,[1] Byung-Jae Kang,[1] Ki-Young Choi,[4] Kyung-Sun Kang,[5] and Heung Myong Woo[1,*]

College of Veterinary Medicine & Institute of Veterinary Science, Kangwon National University, Chuncheon, Gangwon 200-701, Republic of Korea,[1] Department of Medicine, GI Unit, Massachusetts General Hospital and Harvard Medical School, Boston, MA 02114, USA,[2] College of Veterinary Medicine, Chungbuk National University, Cheongju, Chungbuk 28644, Republic of Korea,[3] Department of Controlled Agriculture, Kangwon National University, Chuncheon, Gangwon 200-701, Republic of Korea,[4] and Research Institute for Veterinary Science, College of Veterinary Medicine, Seoul National University, Seoul 08826, Republic of Korea[5]

Received 14 October 2018; accepted 15 February 2019
Available online 21 March 2019

Decellularization of a whole organ is an attractive process that has been used to create 3D scaffolds structurally and micro-architecturally similar to the native one. Currently used decellularization protocols exhibit disrupted extracellular matrix (ECM) structure and denatured ECM proteins. Therefore, maintaining a balance between ECM preservation and cellular removal is a major challenge. The aim of this study was to optimize a multistep Triton X-100 based protocol (either using Triton X-100/ammonium hydroxide mixture alone or after its modification with DNase, sodium dodecyl sulfate or trypsin) that could achieve maximum decellularization with minimal liver ECM destruction suitable for subsequent organ implantation without immune rejection. Based on our findings, Triton X-100 multistep protocol was insufficient for whole liver decellularization and needed to be modified with other detergents. Among all Triton X-100 modified protocols, a Triton X-100/DNase-based one was considered the most suitable. It maintains a gradual but sufficient removal of cells to generate decellularized biocompatible liver scaffolds without any significant alteration to ECM micro- and ultra-structure.

© 2019, The Society for Biotechnology, Japan. All rights reserved.

[**Key words:** Tissue engineering; Biocompatibility; Decellularization; Liver; Triton X-100]

Over recent decades, great progress has been made in the field of tissue engineering. Liver transplantation is considered a promising solution for end stage- and acute liver failure because of organ-donor shortages. Many trials have been carried out in order to obtain 3D, structurally, and micro-architecturally preserved liver scaffolds, either of natural or synthetic origin (1,2). Nevertheless, natural extracellular matrix (ECM)-derived liver scaffolds show superior characteristics over those of synthetic origins in mimicking native ones (3).

The efficiency of the decellularization protocol is organ-specific as it differs according to the organ architecture, organ density and cellularity (4). There are wide varieties of decellularization protocols for solid organs such as the liver, however, using decellularized liver scaffolds in clinical applications was not possible until now due to the complex hepatic microarchitecture that must be fully preserved after decellularization (5). In addition, none of the published protocols provide a complete detailed comparison using different detergents at selected timepoints during decellularization and their conclusions depend mainly on the characterization of the scaffold at the endpoint of each decellularization protocol (6–8). Regarding the decellularizing detergents, previous studies showed that Triton X-100, a nonionic detergent, has been used in decellularizing various tissues and possesses a beneficial effect in preserving ECM integrity, maintaining tissue ultra-structure and limiting ECM protein disruption drawbacks (9). However, previous studies revealed a debate regarding the decellularizing efficiency of Triton X-100 alone or a Triton X-100/ammonium hydroxide mixture in various organs (9–11).

In this study, we used alternative multistep Triton X-100-based protocols, including using Triton X-100 and an ammonium hydroxide mixture alone or in combination with enzymatic action by DNase and trypsin or with ionic detergents such as sodium dodecyl sulfate (SDS). We developed a standardized protocol for liver decellularization, by determining and monitoring the changes that occur in liver micro- and ultrastructure over time during decellularization, and selected the best time point at which the scaffolds reach maximum decellularization with minimal ECM destruction.

MATERIALS AND METHODS

Animals Experiments were performed on 78 C56BL/6 mice (20–24 g, age 4 weeks) for liver harvesting, and on 24 ICR mice (25–30 g, age 5 weeks) for *in vivo* biocompatibility studies in accordance with the regulations of the Institutional Animal Care and Use Committee (Kangwon National University, South Korea).

Liver harvesting After ketamine/xylazine anesthesia, a midventral celiotomy was performed on each mouse. The portal vein was identified and cannulated with a 24-gauge catheter. The whole liver was dissected and flushed with

* Corresponding author at: College of Veterinary Medicine and Stem Cell Institute, Kangwon National University, Hyojadong 192-1, Chuncheon, Gangwon, Republic of Korea. Tel.: +82 33 250 8651/8981; fax: +82 33 244 2367.
E-mail address: woohm@kangwon.ac.kr (H.M. Woo).

1389-1723/$ – see front matter © 2019, The Society for Biotechnology, Japan. All rights reserved.
https://doi.org/10.1016/j.jbiosc.2019.02.007

heparinized PBS to remove remnant blood. Next, livers were connected to a peristaltic pump.

Decellularization with 1% Triton X-100/0.1% ammonium hydroxide As shown in Fig. S1A, livers were decellularized using multi-step alternative perfusions of 1% Triton X-100/0.1% ammonium hydroxide mixture at a flow rate of 4 ml/min. Then washed with PBS for 6 h to remove any residual detergent.

Gross and microscopic examinations with hematoxylin and eosin staining Gross examination of murine livers was carried out and tissue samples from the median lobe of partially decellularized and decellularized livers were taken after each step. Next, liver samples were fixed in 10% neutral buffered formalin, embedded in paraffin, sectioned at 5 μm and stained with hematoxylin and eosin (H&E) staining. Photomicrographic images were taken under light microscope (Olympus, Tokyo, Japan). Here, we focused on one of the largest lobes of livers (which is the median lobe) in order to build a detailed picture regarding the changes that occur during decellularization.

Scanning electron microscopy Samples from native and decellularized livers after different decellularization steps were fixed in 2.5% glutaraldehyde for 24 h at 4°C. Samples were then rinsed with distilled water and dehydrated across a graded ethanol series. Specimens were dried via critical point dryer and mounted on aluminum stubs followed by their coating with Au/Pd. Scanning electron microscopy (SEM) images were recorded at Korea Basic Science Institute, Chuncheon, Korea, using a Carl Zeiss SEM microscope (Carl Zeiss, Oberkochen, Germany).

DAPI-nuclear staining and DNA quantification Paraffin embedded liver tissue sections were stained with nuclear-specific 4,6-diamidino-2- phenylindole (DAPI). Representative images were taken under fluorescent microscope (Olympus). In addition, DNA was isolated using Total DNA Extraction Kit (iNtRON Biotechnology, Kyunggi, Korea) following the manufacturer's protocol. 25 mg of native and decellularized liver was minced and digested with proteinase K in digestion buffer for 4 h. DNA was extracted, purified, and quantified using a Nanodrop spectrophotometer ND-1000 (PeqLab, Erlangen, Germany).

Vascular integrity In order to detect microvascular network patency, trypan blue dye (Sigma Aldrich, St. Louis, MO, USA) was injected through a cannula placed into the portal vein of decellularized scaffolds.

Decellularization with modified 1% Triton X-100/0.1% ammonium hydroxide-based protocols As shown in Fig. 1A–C, livers were decellularized using different modified multi-step 1% Triton X-100/0.1% ammonium hydroxide-based protocols using 30 μg/ml DNase enzyme (TX/DNase group), 0.1% SDS (TX/SDS group), or 0.02% trypsin/0.05% ethylenediaminetetraacetic acid (EDTA) (TX/trypsin group), then washed with PBS for 6 h to remove any residual detergent.

Using the same methodology as that mentioned above, the livers decellularized by modified protocols were examined grossly, histologically, and ultra-structurally. The residual DNA was determined using DAPI staining and DNA quantification. The vascular integrity was examined with trypan blue dye.

Biochemical analyses of the main ECM component Collagen, elastin and sulfated glycosaminoglycans (GAGs) were quantified in native (control) livers and decellularized livers using both a 1% Triton X-100/0.1% ammonium hydroxide mixture without modifications (TX-100 group/blank), and mixtures with different modified groups (tested groups) using Sircol, Fastin and Blyscan assay kits (Biocolor, Ltd., Northern Ireland, UK). Samples were digested and solubilized in pepsin, oxalic acid, and papain for collagen, elastin, and GAGs extraction, respectively, according to the manufacturer's instructions.

Immunofluorescent staining Paraffin sections (5-μm thick) were permeabilized with 0.1% Triton X-100, blocked with 1% goat serum albumin, and incubated overnight at 4°C with the following primary antibodies: polyclonal rabbit anti-collagen I (ab34710), polyclonal rabbit anti-collagen IV (ab19808), polyclonal rabbit anti-laminin (ab11575), polyclonal rabbit anti-fibronectin (ab2413), polyclonal rabbit anti-hepatocyte growth factor (HGF) (ab83760), and polyclonal rabbit anti-vascular endothelial growth factor (VEGF) receptor (ab2350). The slides were then washed, incubated with the corresponding secondary antibody, goat anti-rabbit IgG (Alexa Fluor 647, ab150079), and counterstained with DAPI. All antibodies were purchased from Abcam, UK. Finally, representative images were obtained using a fluorescent microscope (Olympus).

***In vitro* cytocompatibility** *In vitro* cytocompatibility of the decellularized livers of both Triton X-based protocols modified with DNase or SDS was carried out using three different cell types of HepG2 (human hepatocellular carcinoma), EAhy926 (human endothelial), and LX-2 (human hepatic stellate) cell lines that comprise the majority of liver tissue (12). According to previous studies (13,14), conditioned media were prepared by incubation of the decellularized scaffolds from modified protocols utilizing either (TX/SDS or TX/DNase) in serum free DMEM (0.2 g/ml media) (scaffold concentration) at 37°C for 3 days in a shaker at 70 rpm/min. Conditioned media were filtered and stored at 4°C. HepG2, EAhy926 or LX-2 cells were suspended and cultured in DMEM containing 10% fetal bovine serum (FBS) and 1% penicillin-streptomycin and incubated for 24 h at 37°C in 5% CO_2. Next, normal DMEM was replaced by conditioned media from each modified protocol (either TX/SDS or TX/DNase) as well as negative control (normal media) in individual cultures of the three different precultured cell lines separately, after adding 10% FBS and 1% penicillin-streptomycin and positive control (10% DMSO). Cells were incubated again for 24 h. After incubation, cytotoxic effects were determined by indirect 3-(4,5-dimethylthiazol-2-yl)-2,5-diphenyltetrazolium bromide (MTT assay, Sigma-Aldrich, St. Louis, MO, USA) according to the manufacturer's instructions. Optical absorbance was measured at a wavelength of 570 nm using a microplate spectrophotometer.

***In vivo* biocompatibility** Twenty-four ICR mice were divided equally into 4 groups, each of 6 mice. After anesthesia of animals and preoperative aseptic preparation of the surgical fields, subcutaneous implantation of native and decellularized scaffolds was carried out in the dorsum region, following previous studies (12,15). A small incision was created (5 mm) followed by blunt dissection to form a subcutaneous pocket. Native or decellularized liver discs (obtained by a biopsy punch tool with 6 mm diameter) of the Triton X-based protocols modified with DNase or SDS were inserted into the subcutaneous pocket. In the sham group, the surgical operation was conducted without implantation of any scaffold to exclude any alterations that might have resulted from the surgical procedure itself (16,17). The wound was closed traditionally, and all animals were observed for any signs of infection involving the surgical wound. Three mice were sacrificed from each group at each time point (7 and 21 days) post-implantation (PI). Samples from implants and the surrounding area were collected for examination. H&E staining of the samples was performed. Samples were fixed in 10% neutral buffered formalin and processed for routine histological evaluation. Qualitative analysis of the histologically stained slides was carried out under light microscopy to determine the degree and type of inflammatory cell infiltration. In addition, quantitative analysis of the infiltrated inflammatory cells (neutrophils and lymphocytes) was performed by counting 5 different fields (at × 200 magnification) for each slide.

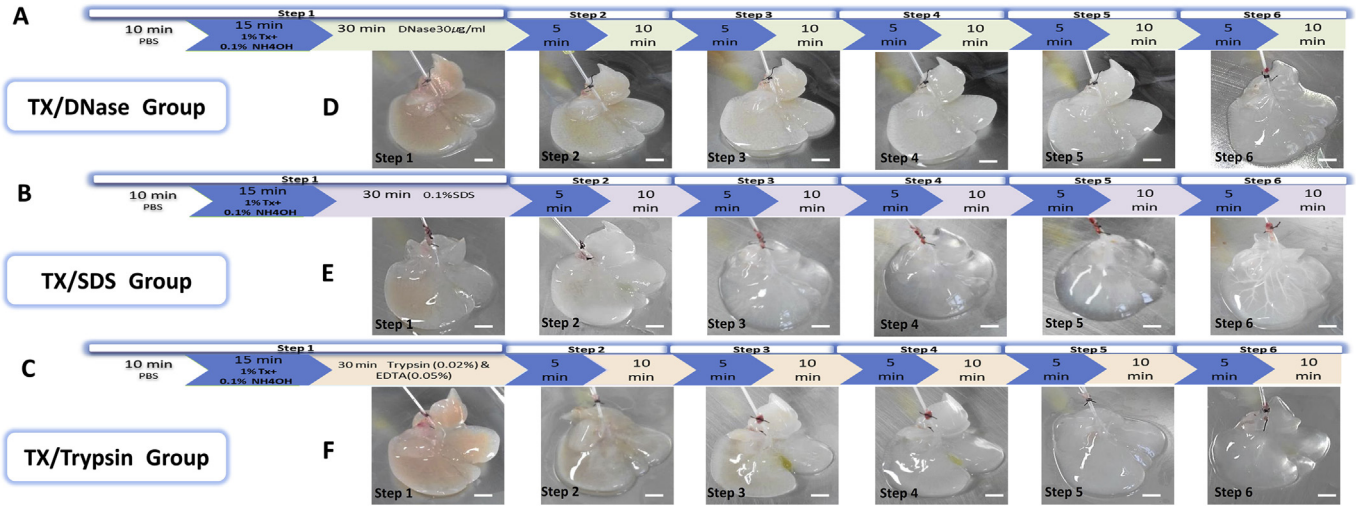

FIG. 1. Schema of the modified multistep Triton X-100-based protocols (A–C) and their macroscopic appearances (D–F). (A, D) TX/DNase, (B, E) TX/SDS, and (C, F) TX/trypsin.

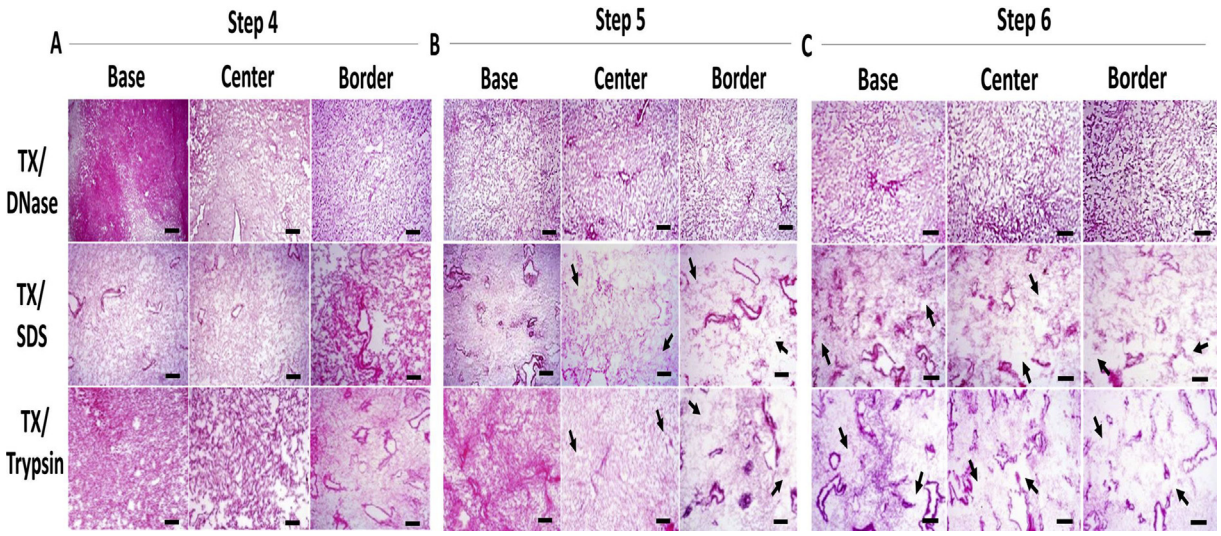

FIG. 2. Representative microscopic images of different parts of the median lobe (base, center and border) via H&E staining after steps 4 (A), 5 (B), and 6 (C) of the modified multistep Triton X-100-based protocols (TX/DNase, TX/SDS and TX/trypsin). Arrows indicate areas of ECM destruction. Scale bar: 100 μm.

Immunofluorescent staining was also performed to determine macrophage phenotype. The primary antibodies used were anti-CD68 (pan macrophage marker) (Alexa Fluor 405) (ab199571, abcam, UK) (data not shown), anti-CCR7 (M1 macrophage marker) (Alexa Fluor 555) (ab207018, abcam, UK), and anti-CD206 (M2 macrophage marker) (Alexa Fluor 594) (no. 141726, Bio-legend, CA, USA). DAPI was used as a nuclear counter stain. Representative images were taken at 7 and 21 days PI by fluorescent photomicroscopy. M1 and M2 polarization was quantified using ImageJ analysis software version 1.47. M1% was calculated by dividing the number of M1 immunopositive cells by the number of the pan macrophages in each field. Similarly, M2% was calculated by dividing the number of M2 immunopositive cells by the number of pan macrophages in each field. These percentages were expressed as M1/M2 ratios.

Statistical analysis Univariate analysis of variance (ANOVA) with an honest significant difference (HSD)–Tukey *post hoc* multiple comparison test was performed for comparisons among the different groups. All tests were performed using the statistical software program SPSS version 21.

RESULTS

Characterization of scaffolds decellularized by multistep Triton X-100 protocol Gross findings of liver scaffolds during the perfusion of Triton X-100 and ammonium hydroxide mixture revealed that liver scaffolding attained a translucent coloration by the end of step 4 (Fig. S1B). Microscopic examination after H&E staining showed that the decellularization process begins slowly from the borders of the median lobe and increases gradually toward the center and the base. Even after step 6, liver scaffolds showed the presence of retained cytoplasmic debris. In addition, ECM at the border of scaffolds showed multiple scattered areas of destruction (Fig. S1C). This histological finding was also confirmed by SEM imaging where collagen fibers showed discrete disruption, especially at the borders of the lobe (Fig. S2). Residual nuclear content was demonstrated by using DAPI staining, as shown in Fig. S3A. Regarding the quantitative analysis of DNA content by Nanodrop spectrophotometry, the results showed that the DNA remaining after step 6 was 25.5 ± 3.8% that of the native scaffold (Fig. S3B). Native vascular integrity was identified by portal perfusion of trypan blue dye. Triton X-100 was found to be unable to maintain the vascular integrity of the finest blood vessels (Fig. S3C). Accordingly, complete cellular removal without structural destruction was not obtained by using the Triton X-100 and ammonium solution mixture. Consequently, we modified this protocol by adding three different detergents of different efficiencies in order to trigger the Triton X-100 decellularizing efficiency with no (or minimal) deleterious effects on ECM structure.

Gross, micro- and ultrastructural changes of liver scaffolds decellularized with different modified multistep Triton X-100 protocols during the decellularization process Macroscopically, liver scaffolds were observed to reflect differences in decellularization efficiencies among the different modified Triton X-100-based protocols. TX/SDS-treated liver scaffolds attained a completely translucent appearance after step 2, while in TX/DNase and TX/trypsin, translucent coloration of scaffolds occurred after step 4 (Fig. 1D–F).

As shown in Figs. 2 and S4, microscopic appearance by H&E revealed that complete disappearance of cellular remnants occurred at steps 4, 5, and 6 in TX/SDS, TX/DNase and TX/trypsin, respectively. Regarding ECM integrity, the TX/DNase decellularization protocol showed improved preservation of ECM architecture even after step 6. However, minimal ECM damage was identified at the border of the scaffold after step 4 of the TX/SDS protocol and obvious ECM destruction after steps 5 and 6. Similarly, the TX/trypsin protocol resulted in severe ECM breakdown starting from step 4. The findings of the microscopic examination were also confirmed by SEM imaging, as shown in Figs. 3 and S5.

Qualitative and quantitative assessments of residual DNA from liver scaffolds decellularized with different modified multistep Triton X-100 protocols at selected timepoints during decellularization Qualitative assessment of nuclear residue observed via DAPI staining is shown in Fig. 4A, which confirmed the absence of nuclear content from both TX/DNase and the TX/trypsin modified groups after step 6 in contrast to TX/SDS where nuclear content qualitatively disappeared after step 2. DNA quantification was carried out to check the efficiencies of the different modified decellularization protocols. The TX/SDS protocol resulted in a rapid reduction in DNA content that reached 4.2 ± 1.1% after step 4 and 2.2 ± 0.6% after step 6, in comparison to the native scaffold DNA. The other decellularization protocols exhibited a gradual decrease in DNA content. The residual DNA content in the TX/DNase and the TX/trypsin protocols were 4.7 ± 0.4% and 17.0 ± 5.2%, respectively, after step 6 compared to native scaffolds (Fig. 4B).

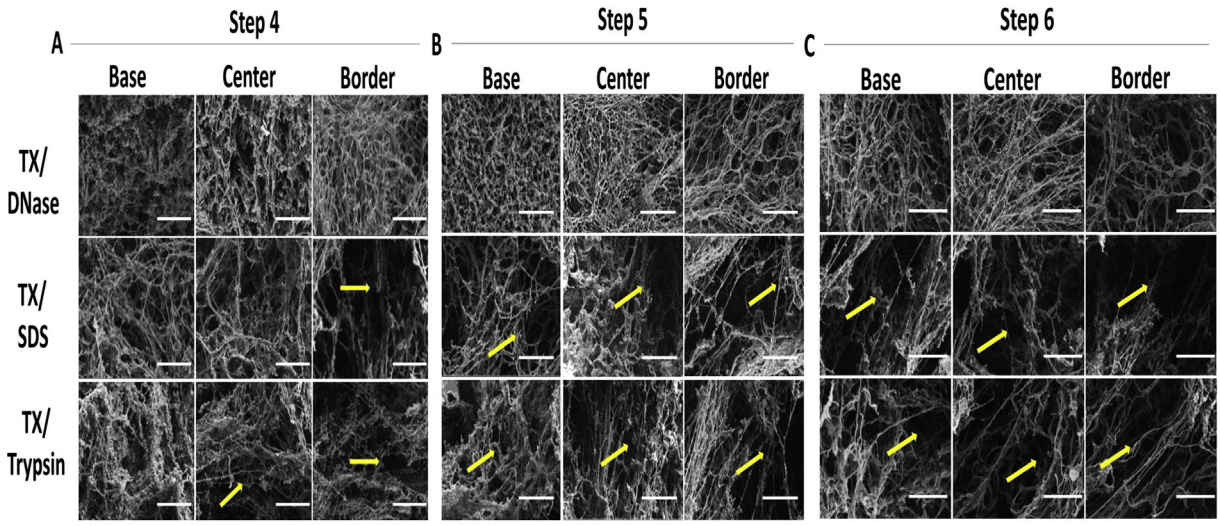

FIG. 3. Ultra-structural analysis using SEM of different parts of the median lobe (base, center, and border) after steps 4 (A), 5 (B), and 6 (C) of the modified multistep Triton X-100-based protocols (TX/DNase, TX/SDS and TX/trypsin). TX/DNase protocols showing a completely decellularized scaffold with preserved ECM. Arrows indicate areas of ECM destruction. Scale bar: 30 μm.

Further comparisons were carried out between TX/DNase (step 6) and TX/SDS (step 4), based on the presence of a high degree of cell removal and minimal ECM destruction as assessed by histological and ultrastructural analyses, DAPI staining and DNA quantification. The TX/trypsin decellularization protocol was omitted from further analyses as it showed insufficient decellularization as well as high levels of ECM destruction.

Liver matrix vasculature integrity of both TX/DNase and TX/SDS modified protocols Portal perfusion of trypan blue dye elucidated that the TX/DNase protocol resulted in well-preserved and intact microvasculature in contrast to that observed in the TX/SDS protocol, which showed vascular leakage and discontinuities (Fig. 4C).

Qualitative and quantitative assessments of ECM proteins and growth factors from both TX/DNase and TX/SDS modified protocols Biochemical analyses of ECM components showed no significant differences ($P \geq 0.05$) among the collagen contents of all groups. In addition, although the different decellularized groups showed significant losses ($P < 0.05$) in elastin and GAGs contents compared to the native group, the TX/SDS group showed the highest loss with significant differences ($P < 0.05$) compared to the TX and TX/DNase groups. Moreover, there were no significant differences ($P \geq 0.05$) between the TX and TX/DNase groups, which revealed that modifying the TX group with DNase had no additional deleterious effects on ECM components (Fig. S6).

The immunofluorescent staining qualitatively indicated retention of ECM-bound growth factors (VEGF and HGF) and ECM

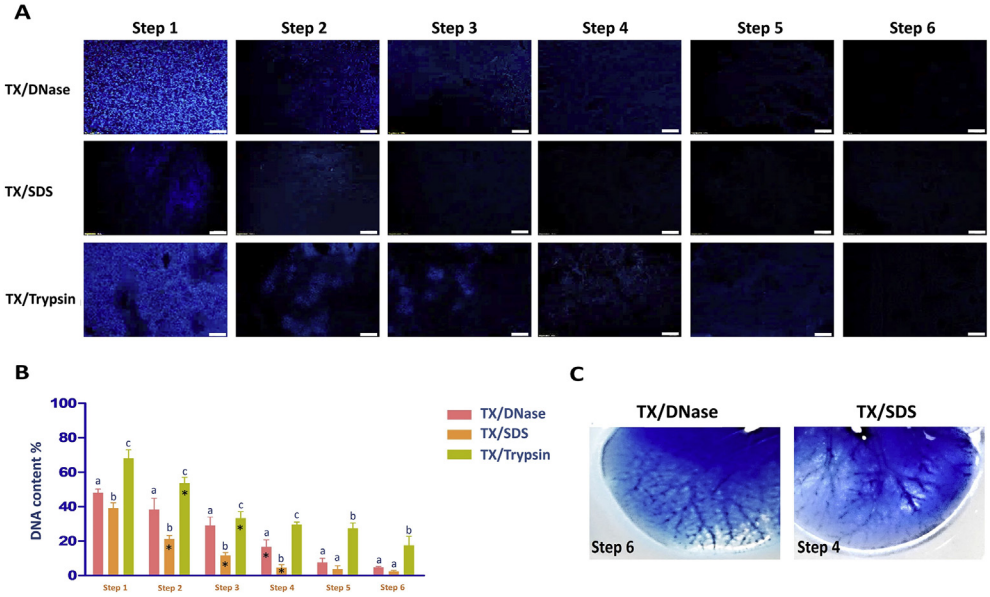

FIG. 4. (A) Qualitative assessment of nuclear content of scaffolds via DAPI staining in different steps of modified Triton X-100 based decellularization protocols. Scale bar: 100 μm. (B) DNA quantification using Nanodrop spectrophotometry in different modified Triton X-100 based decellularization protocols at different steps. Different letters indicate significant differences ($P < 0.05$) among different groups for the same steps. Asterisks (*) indicate significant differences ($P < 0.05$) among different steps in the same group. (C) Representative images of decellularized median lobes using modified Triton X-100 protocols after trypan blue portal perfusion.

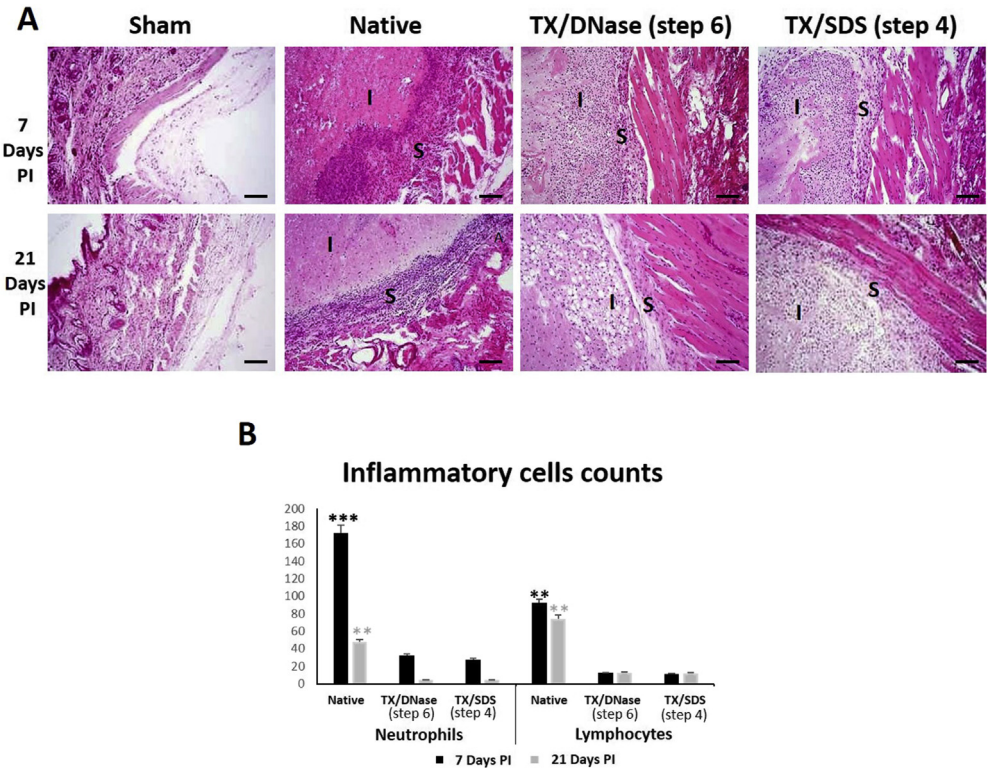

FIG. 5. *In vivo* host immune responses directed towards the implanted scaffolds decellularized by TX/DNase (step 6) and TX/SDS (step 4) protocols. (A) Qualitatively by H&E stained tissue sections including the implanted scaffolds and surrounding areas. Scale bar: 100 μm. (B) Quantitatively by counting the number of infiltrating neutrophils and lymphocytes in 5 different fields at 7 and 21 days PI. Black asterisks indicate significant differences ($P < 0.01^{**}$ and $P < 0.001^{***}$) at 7 days, while grey asterisks indicate significant differences ($P < 0.01^{**}$) at 21 days.

proteins (fibronectin and laminin) in the scaffolds treated with TX/DNase protocol, than those subjected to the TX/SDS protocol. While collagen I and IV showed similar expressions in the two groups (Fig. S7).

***In vitro* cytocompatibility and *in vivo* host immune response for both TX/DNase and TX/SDS modified protocols** Cell viability was checked, and we noted that both decellularization protocols exerted no cytotoxic effects on the three different cell types (HepG2, EAhy926, LX-2), which indicated that scaffolds were adequately flushed free of any detergent residue by prolonged washing (Fig. S8).

The host immune response toward the implanted scaffolds showed dense infiltration by neutrophils and mononuclear inflammatory cells around the native discs 7 days PI. The results of the sham group showed that the surgical procedure did not produce any undesirable inflammatory effects at either 7 or 21 days post-operation. The native group showed the most intense response with significant differences ($P < 0.001$ and $P < 0.01$) when compared to both decellularization groups at 7 and 21 days PI, respectively. At 21 days PI, there was a reduction in the total number of inflammatory cells inform of randomly infiltrated inflammatory cell and organized connective tissue surrounding the implanted scaffolds with degradation of the implanted scaffolds. The decellularized implanted scaffolds in TX/SDS and TX/DNase protocols showed that the number of inflammatory cells was greatly reduced with no significant differences ($P \geq 0.05$) at either days 7 or 21 PI (Fig. 5).

The results of immunofluorescence staining showed that infiltration by mononuclear macrophages was detected mostly in the area around the implanted scaffold. In the native scaffold group, M1 macrophages were the predominate phenotype. However, the TX/SDS and TX/DNase groups showed a predominance of M2 phenotype macrophages at both days 7 and 21 PI (Fig. 6A). These findings were confirmed by calculating M1/M2 ratios, which also showed that there were no significant differences ($P \geq 0.05$) between the TX/SDS and TX/DNase groups (Fig. 6B). Our results confirmed that the implanted scaffolds from both decellularization protocols were biocompatible and showed no immune rejection.

DISCUSSION

In this study, we succeeded in standardizing a gentle decellularization protocol for mouse liver. To the best of our knowledge, this is the first study that monitors the micro- and ultrastructural changes of liver ECM during decellularization to achieve an adequate level of cellular removal, which is essential to avoid adverse immune responses as well as to maintain ECM structural integrity as far as possible. Accordingly, we used low rate perfusion of a Triton X-100 multistep-based protocol as Triton X-100 is considered to be a gentle decellularizing non-ionic detergent previously used in decellularization of various organs and has no harsh effects on liver ECM (18).

Although Triton X-100 could preserve ECM proteins, our gross and histological findings in scaffolds during the decellularization process revealed that perfusion of 1% Triton X-100/0.1% ammonium hydroxide mixture led to insufficiently slow release of cellular and nuclear contents, which resulted in non-homogenous and incompletely decellularized scaffolds.

Histological and ultrastructural analyses showed persistent cytoplasmic remnants as well as damaged ECM. By quantitating DNA content, our results showed that Triton X-100/ammonium hydroxide mixture removed only approximately 74.5% of native DNA. All of these findings could be interpreted by the low ability of such mixture in removing cellular residue, especially in compact

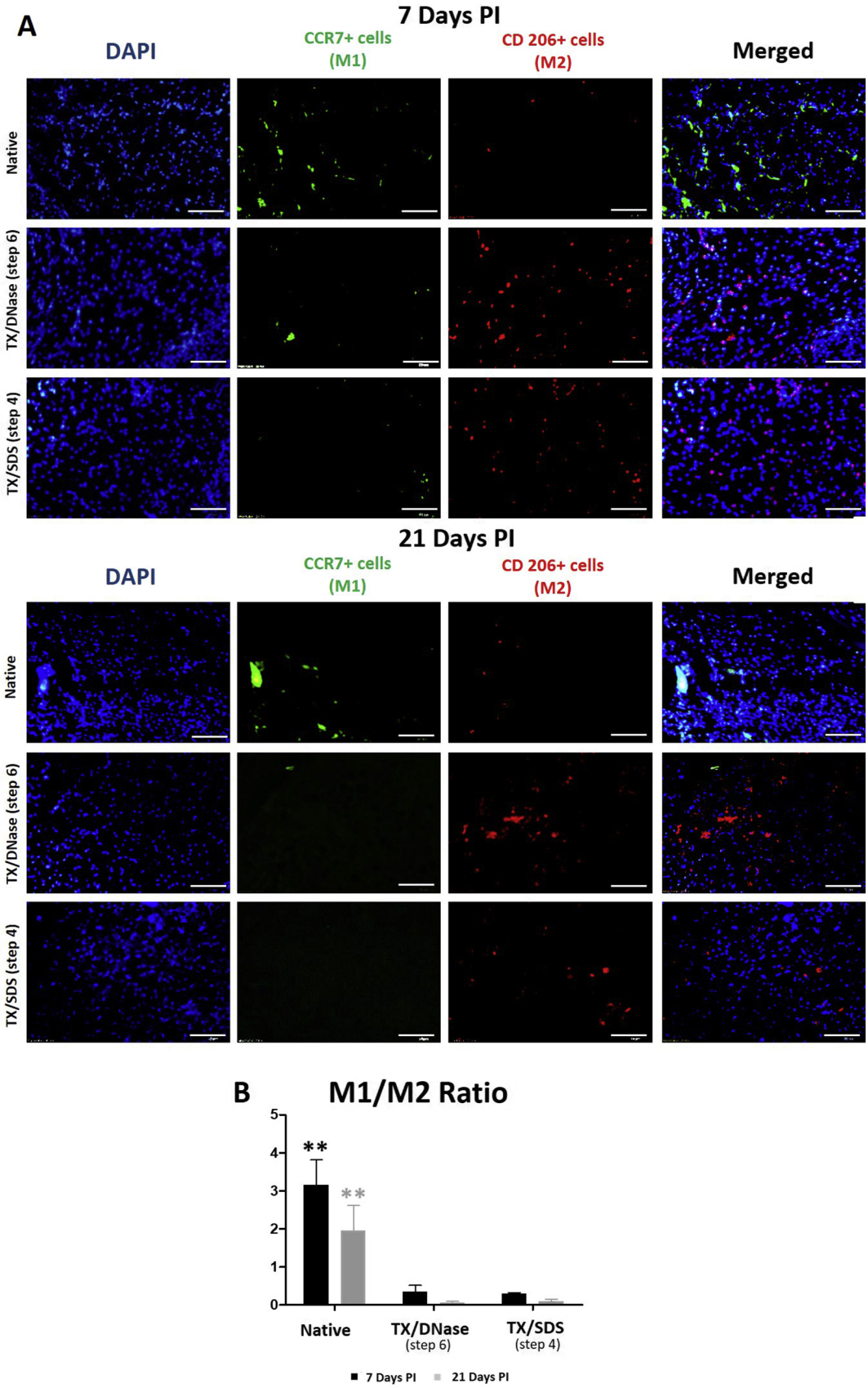

FIG. 6. (A) Immunofluorescent staining for M1 and M2 macrophage polarization at 7 and 21 days post implantation of scaffolds decellularized by TX/DNase (step 6) and TX/SDS (step 4) protocols. Scale bar: 50 μm. (B) M1:M2 ratio for scaffolds decellularized by TX/DNase and TX/SDS protocols. Black asterisks mean indicate significant differences ($P < 0.01^{**}$) at 7 days, while grey asterisks indicate significant differences ($P < 0.01^{**}$) at 21 days.

organs. In addition, the high molecular weight of Triton X-100 may result in structural damage to liver scaffolds (19,20). On the contrary, other studies indicated that Triton X-100 successfully decellularized various non-parenchymatous organs (e.g., small intestine, thoracic aorta) while maintaining intact 3D ECM structures (21,22). From our results, using Triton X-100 in decellularization of compact parenchymatous organs such as the liver must be incorporated with alternative multistep perfusion by another detergent that triggers and powers its decellularizing effect, as well as facilitating the removal of residual Triton X-100 detergent.

Herein, we modified the Triton X-100-based decellularization protocol by adding DNase, SDS or trypsin. The microscopic appearance of different parts of the median lobe varied according to cellular densities because the base of the scaffold requires much more time to reach complete decellularization compared to the border, even if they have the same translucent appearance grossly. The histological and ultrastructural analyses demonstrated that the TX/DNase protocol was the best in removing all cellular components without affecting ECM architecture, whereas the fastest protocol for obtaining acellular scaffolds was the TX/SDS protocol with ECM alteration especially at the latter stages of decellularization. In addition, the TX/trypsin protocol exhibited the lowest decellularizing efficiency and had the most deleterious effects on ECM among the suggested modified protocols.

Consequently, we selected the step of choice from both decellularizing strategies (TX/DNase, TX/SDS) and omitted the TX/trypsin protocol in which trypsin was confirmed to be inappropriate for liver decellularization as indicated in previous studies (23,24).

Regarding the vascular patency and the preservation of ECM components, TX/DNase was found to be the best protocol in retaining ECM proteins and preserving the vascular network.

In addition, the TX/DNase-decellularized tissue preserved much higher quantities of ECM bound growth factors, which play important roles in the attachment and proliferation of hepatocytes and endothelial cells (25).

Because the evaluation of cytocompatibility is essential to ensure the possibility of further transplantation of biomaterials (13), testing of *in vitro* cytocompatibility was performed in this study using different kinds of cells that comprise a majority of the liver tissue. The generated scaffolds from either TX/DNase and TX/SDS had no cytotoxic effects.

The efficiency of decellularization of TX/DNase and TX/SDS protocols was also evaluated by determining the local host immune response towards the different subcutaneously implanted decellularized scaffolds. Qualitative and quantitative analyses of histological sections resulting from TX/DNase and TX/SDS protocols at 7 days PI represent the period of early inflammatory reactions during which the implanted scaffolds resulted in release of inflammatory cytokines which in turn led to recruitment of neutrophil and mononuclear inflammatory cells toward the implant sites (26,27). Late immune responses were observed at 21 days PI, when there was a significant decrease in the numbers of inflammatory cells with both decellularization protocols. However, there were no significant differences in the numbers of inflammatory cells with the TX/DNase and TX/SDS protocols at 7 and 21 days PI. By analyzing macrophage phenotype polarization, the TX/DNase and TX/SDS protocols showed M2 macrophage polarization, which indicates tissue regenerative responses are promoted with either protocol (28). The inclusion of SDS and DNase in the Triton X-100-based protocol significantly removed cellular contents leaving complete acellular scaffolds with significantly lower immunogenicity. However, SDS caused ECM structural alterations. Similar findings were reported in the study of Du et al. (29), who indicated that using SDS in decellularization alters ECM microarchitecture, whereas the studies of Caralt et al. (10) and Sabetkish et al. (30) had results contradictory to ours as they mentioned that including SDS in decellularization protocols assisted rapid and complete decellularization with none or little ECM damage. In our study, DNase was superior to SDS in maintaining a well-preserved 3D porous microarchitecture of liver tissue. These findings can be interpreted by the ability of DNase enzymes in facilitating the removal of DNA agglutination found to be attached to the scaffold ECM when added to the decellularization protocols, and also may assist in the gradual washing out of Triton X-100 from the scaffold (31,32). In contrary, the study by Shirakigawa et al. (33) stated that decellularization of liver by using higher concentration of Triton X-100 (4%) followed by DNase gave rise to scaffolds with rough ECM, as visualized by SEM.

This study concluded that six steps of low-rate multi-step alternative perfusions of Triton X-100 (1%)/ammonium hydroxide (0.1%) and DNase enzyme (30 μg/ml) (TX/DNase protocol) was sufficient to adequately decellularize murine liver tissue, with well-preserved cyto- and biocompatible ECMs. This provides a naturally-derived 3D microenvironment for cell growth and proliferation for subsequent liver transplantation.

Supplementary data to this article can be found online at https://doi.org/10.1016/j.jbiosc.2019.02.007.

ACKNOWLEDGMENTS

This work was supported by “Cooperative Research Program for Agriculture Science & Technology Development” (Project No. PJ01100201), Rural Development Administration, Republic of Korea.

The authors certify to have no conflict of interest.

Ebtehal Ahmed designed and performed the research experiments, data analysis/interpretation and wrote the manuscript; Tarek Saleh, Yu-Lina, Ho-Hyun Kwak, Byeong-Moo Kim, Kyung-Mee Park, Yun-Suk Lee, Byung-Jae Kang, and Ki-Young Choi contributed to data discussion. Kyung-Sun Kang involved in financial support, and final approval of manuscript. Heung Myong Woo participated in study design, interpretation of data, and the approval of the article and secured funding.

References

1. **Ren, H., Shi, X., Tao, L., Xiao, J., Han, B., Zhang, Y., Yuan, X., and Ding, Y.:** Evaluation of two decellularization methods in the development of a whole-organ decellularized rat liver scaffold, Liver Int., **33**, 448–458 (2013).
2. **Shim, J.-H., Kim, J. Y., Park, M., Park, J., and Cho, D.-W.:** Development of a hybrid scaffold with synthetic biomaterials and hydrogel using solid freeform fabrication technology, Biofabrication, **3**, 034102 (2011).
3. **Bishi, D. K., Mathapati, S., Venugopal, J. R., Guhathakurta, S., Cherian, K. M., Ramakrishna, S., and Verma, R. S.:** Trans-differentiation of human mesenchymal stem cells generates functional hepatospheres on poly (L-lactic acid)-*co*-poly (ε-caprolactone)/collagen nanofibrous scaffolds, J. Mater. Chem. B, **1**, 3972–3984 (2013).
4. **Keane, T. J., Swinehart, I. T., and Badylak, S. F.:** Methods of tissue decellularization used for preparation of biologic scaffolds and in vivo relevance, Methods, **84**, 25–34 (2015).
5. **Morini, S., Sánchez-Romero, N., Palacín, I. P., Arnal, P. S., Almeida, M., Verscheijden, L., Almeida, J. I., Lue, A., Llorente, S., and Almeida, H.:** Liver tissue engineering, pp. 301–327, in: Claudia, L. (Ed.), Bioreactors for stem cell expansion and differentiation. CRC Press (2018).
6. **Shupe, T., Williams, M., Brown, A., Willenberg, B., and Petersen, B. E.:** Method for the decellularization of intact rat liver, Organogenesis, **6**, 134–136 (2010).
7. **Uygun, B. E., Soto-Gutierrez, A., Yagi, H., Izamis, M.-L., Guzzardi, M. A., Shulman, C., Milwid, J., Kobayashi, N., Tilles, A., and Berthiaume, F.:** Organ reengineering through development of a transplantable recellularized liver graft using decellularized liver matrix, Nat. Med., **16**, 814 (2010).
8. **White, L. J., Taylor, A. J., Faulk, D. M., Keane, T. J., Saldin, L. T., Reing, J. E., Swinehart, I. T., Turner, N. J., Ratner, B. D., and Badylak, S. F.:** The impact of detergents on the tissue decellularization process: a ToF-SIMS study, Acta Biomater., **50**, 207–219 (2017).
9. **Zhou, P., Guo, Y., Huang, Y., Zhu, M., Fan, X., Wang, L., Wang, Y., Zhu, S., Xu, T., and Wu, D.:** The dynamic three-dimensional culture of islet-like clusters in decellularized liver scaffolds, Cell Tissue Res., **365**, 157–171 (2016).

10. **Caralt, M., Uzarski, J. S., Iacob, S., Obergfell, K. P., Berg, N., Bijonowski, B. M., Kiefer, K. M., Ward, H. H., Wandinger-Ness, A., and Miller, W. M.:** Optimization and critical evaluation of decellularization strategies to develop renal extracellular matrix scaffolds as biological templates for organ engineering and transplantation, Am. J. Transplant., **15**, 64–75 (2015).
11. **Fischer, I., Westphal, M., Rossbach, B., Bethke, N., Hariharan, K., Ullah, I., Reinke, P., Kurtz, A., and Stachelscheid, H.:** Comparative characterization of decellularized renal scaffolds for tissue engineering, Biomed. Mater., **12**, 045005 (2017).
12. **Mazza, G., Rombouts, K., Hall, A. R., Urbani, L., Luong, T. V., Al-Akkad, W., Longato, L., Brown, D., Maghsoudlou, P., and Dhillon, A. P.:** Decellularized human liver as a natural 3D-scaffold for liver bioengineering and transplantation, Sci. Rep., **5**, 13079 (2015).
13. **Saleh, T., Ahmed, E., Yu, L., Hussein, K., Park, K.-M., Lee, Y.-S., Kang, B.-J., Choi, K.-Y., Choi, S., and Kang, K.-S.:** Silver nanoparticles improve structural stability and biocompatibility of decellularized porcine liver, Artif. Cells Nanomed. Biotechnol., **46**, 273–284 (2018).
14. **Hussein, K. H., Park, K. M., Teotia, P. K., Hong, S. H., Yang, S. R., Park, S. M., Ahn, C., and Woo, H. M.:** Sterilization using electrolyzed water highly retains the biological properties in tissue-engineered porcine liver scaffold, Int. J. Artif. Organs, **36**, 781–792 (2013).
15. **Piccoli, M., Urbani, L., Alvarez-Fallas, M., Franzin, C., Dedja, A., Bertin, E., Zuccolotto, G., Rosato, A., Pavan, P., and Elvassore, N.:** Improvement of diaphragmatic performance through orthotopic application of decellularized extracellular matrix patch, Biomaterials, **74**, 245–255 (2016).
16. **Koch, H., Graneist, C., Emmrich, F., Till, H., Metzger, R., Aupperle, H., Schierle, K., Sack, U., and Boldt, A.:** Xenogenic esophagus scaffolds fixed with several agents: comparative in vivo study of rejection and inflammation, Bio-Med Res. Int., **2012**, 948320 (2012).
17. **Mirmalek-Sani, S.-H., Sullivan, D. C., Zimmerman, C., Shupe, T. D., and Petersen, B. E.:** Immunogenicity of decellularized porcine liver for bioengineered hepatic tissue, Am. J. Pathol., **183**, 558–565 (2013).
18. **Xu, H., Xu, B., Yang, Q., Li, X., Ma, X., Xia, Q., Zhang, Y., Zhang, C., Wu, Y., and Zhang, Y.:** Comparison of decellularization protocols for preparing a decellularized porcine annulus fibrosus scaffold, PLoS One, **9**, e86723 (2014).
19. **Hrebíková, H., Voborníková, M., Hetešová, M., and Mokrý, J.:** Histological evaluation of decellularized skeletal muscle tissue using two different decellularization agents, Acta Med. (Hradec Kralove), **59**, 107–112 (2016).
20. **Ye, X., Wang, H., Gong, W., Li, S., Li, H., Wang, Z., and Zhao, Q.:** Impact of decellularization on porcine myocardium as scaffold for tissue engineered heart tissue, J. Mater. Sci. Mater. Med., **27**, 70 (2016).
21. **Zou, Y. and Zhang, Y.:** Mechanical evaluation of decellularized porcine thoracic aorta, J. Surg. Res., **175**, 359–368 (2012).
22. **Oliveira, A. C., Garzón, I., Ionescu, A. M., Carriel, V., de la Cruz Cardona, J., González-Andrades, M., del Mar Pérez, M., Alaminos, M., and Campos, A.:** evaluation of small intestine grafts decellularization methods for corneal tissue engineering, PLoS One, **8**, e66538 (2013).
23. **Wang, H., Lin, X.-F., Wang, L.-R., Lin, Y.-Q., Wang, J.-T., Liu, W.-Y., Zhu, G.-Q., Braddock, M., Zhong, M., and Zheng, M.-H.:** Decellularization technology in CNS tissue repair, Expert Rev. Neurother., **15**, 493–500 (2015).
24. **Wang, F., Zhang, J., Wang, R., Gu, Y., Li, J., and Wang, C.:** Triton X-100 combines with chymotrypsin: a more promising protocol to prepare decellularized porcine carotid arteries, Bio Med. Mater. Eng., **28**, 531–543 (2017).
25. **Reynaert, H., Chavez, M., and Geerts, A.:** Vascular endothelial growth factor and liver regeneration, J. Hepatol., **34**, 759–761 (2001).
26. **Jeinsen, N., Mägel, L., Jonigk, D., Klingenberg, M., Haverich, A., Wilhelmi, M., and Böer, U.:** Biocompatibility of intensified decellularized equine carotid arteries in a rat subcutaneous implantation model and in a human in vitro model, Tissue Eng. Part A, **24**, 310–321 (2018).
27. **Badylak, S. F.:** Decellularized allogeneic and xenogeneic tissue as a bioscaffold for 7regenerative medicine: factors that influence the host response, Ann. Biomed. Eng., **42**, 1517–1527 (2014).
28. **Scatena, M., Eaton, K. V., Jackson, M. F., Lund, S. A., and Giachelli, C. M.:** Macrophages: the bad, the ugly, and the good in the inflammatory response to biomaterials, pp. 37–62, in: Corradetti, B. (Ed.), The immune response to implanted materials and devices. Springer (2017).
29. **Du, L., Wu, X., Pang, K., and Yang, Y.:** Histological evaluation and biomechanical characterisation of an acellular porcine cornea scaffold, Br. J. Ophthalmol., **95**, 410–414 (2011).
30. **Sabetkish, S., Kajbafzadeh, A. M., Sabetkish, N., Khorramirouz, R., Akbarzadeh, A., Seyedian, S. L., Pasalar, P., Orangian, S., Beigi, R. S. H., and Aryan, Z.:** Whole-organ tissue engineering: decellularization and recellularization of three-dimensional matrix liver scaffolds, J. Biomed. Mater. Res. A, **103**, 1498–1508 (2015).
31. **Syed, O., Walters, N. J., Day, R. M., Kim, H.-W., and Knowles, J. C.:** Evaluation of decellularization protocols for production of tubular small intestine submucosa scaffolds for use in oesophageal tissue engineering, Acta Biomater., **10**, 5043–5054 (2014).
32. **Wagner, D. E., Bonenfant, N. R., Parsons, C. S., Sokocevic, D., Brooks, E. M., Borg, Z. D., Lathrop, M. J., Wallis, J. D., Daly, A. B., and Lam, Y. W.:** Comparative decellularization and recellularization of normal versus emphysematous human lungs, Biomaterials, **35**, 3281–3297 (2014).
33. **Shirakigawa, N., Ijima, H., and Takei, T.:** Decellularized liver as a practical scaffold with a vascular network template for liver tissue engineering, J. Biosci. Bioeng., **114**, 546–551 (2012).